Journal of Applied Polymer Science

Mechanical, rheological, and electrical properties of multiwalled carbon nanotube reinforced ASA/Na-ionomer blend

Pulak Datta,[1] Chandan Guha,[2] Gautam Sarkhel[1]

[1]Department of Chemical Engineering & Technology, Birla Institute of Technology, Mesra, Ranchi, India

[2]Department of Chemical Engineering, Jadavpur University, Kolkata, India

Correspondence to: G. Sarkhel (E-mail: gautamsarkhel@bitmesra.ac.in)

ABSTRACT: Varying amounts of multiwalled carbon nanotubes (MWCNTs) was melt-extruded with the acrylonitrile-styrene-acrylate (ASA)/Na-ionomer blend, and mechanical, rheological, and electrical properties were studied Optical micrographs show good dispersion level at low MWCNT content and network formation at higher nanotubes percentage. DC conductivity model data shows percolation threshold reached at 1% MWCNT content and after percolation, two-dimensional network structure was formed. The "peak and valley" type surface topology of matrix may be responsible for low percolation threshold limit. The polymer/nanotubes interactions at low MWCNT content increased the mechanical strengths, which were reduced by the network structure and agglomerates of nanotubes at higher nanotubes content. The MWCNTs interacted differently with the architecturally complex polymer chains and controlled chain dynamics accordingly. The Carreau-Yasuda model was found fit to viscosity data and the model parameters data suggest the zero shear viscosity is function of MWCNTs content but the infinite shear viscosity is independent of nanoparticles content.
 J. Appl. Polym. Sci. **2015**, *132*, 42516.

KEYWORDS: composites; dielectric properties; graphene and fullerenes; monolayers and polymer brushes; nanotubes; rheology

Received 21 October 2014; accepted 19 May 2015

DOI: 10.1002/app.42516

INTRODUCTION

After the discovery of carbon nanotubes (CNT) in 1991, the unique combination of exceptionally high mechanical properties (both strength and modulus), thermal properties, and electrical properties have attracted huge activity in the field of material science and engineering.[1–4] One of the major reasons for this unique combination of properties is the high aspect ratio, which is due to the combination of diameters in the nanometer scale, and the unique atomic structure of CNTs. This extraordinary high aspect ratio has also made the CNT-based nanocomposite to achieve lower electrical percolation thresholds compared with many other conventional types of filler.[5–7]

Ionomers are special class of engineered polymers that contain both electrically neutral and partially ionized (generally less than 15%) repeating units.[8–10] The ionic groups form the nanometer-sized ionic aggregates, which strongly control ionomer's flowability and impart high stiffness and toughness. In addition, good abrasion resistance, optical clarity, antistatic properties, interactions with different types of fillers, heat sealability, and adhesion properties with different types of materials like polymers, ceramic, metals, etc.[11,12] make the ionomer a potential polymer in several applications like fuel cell membranes, toughening of epoxy,[13] shape memory material,[14] self-healing material[15] to name a few. The ionic aggregates are distributed within the nonpolar polymer matrix, and at room temperature, form temporary cross-links, which become labile on heating. Commercially available ionomer like Surlyn from DuPont is a copolymer of electrically neutral ethylene units and polar methacrylic acids, where the acid groups are partially neutralized (15–80%) by suitable alkali to form metal salts.

Acrylonitrile-styrene-acrylate (ASA), a triblock copolymer, is an important weather resistant polymer from styrenic families. The inherent weather resistance comes from the saturated acrylate rubber, which replaces the unsaturated butadiene rubber used in more traditionally available acrylonitrile-butadiene-styrene (ABS) terpolymer. In addition, ASA has high thermal stability, resistance to yellowing, good chemical resistance, high impact resistance, and stiffness. Electronics and telecommunication sectors, automotive sectors, etc. are the areas where ASA is used as housing material because of its combination of excellent outdoor and toughness properties. The research activity on ASA and its blend systems are less, and commercial success is mainly limited to few blend systems like ASA/polycarbonate (PC), ASA/polybutylene terephthalate (PBT) and ASA/PC/polymethyl methacrylate (PMMA) blends.[16] Different phase compatibilizers like polycarbonate PC-block-PMMA,[17] PC-graft-styrene

acrylonitrile (SAN),[18] maleic anhydride,[19] diblock copolymer; composed of tetramethyl polycarbonate and PMMA[20] etc. was examined.

The advantages of ionomer like ionic character, antistatic property, and metal adhesion have encouraged Datta *et al.* to study the ASA/Na-ionomer[21,22] blend and ASA/Zn-ionomer blend.[23,24] The ionomer chains are physically attached on the polyacrylate rubber phase of ASA because of similar types of chemical structure of Zn-ionomer and Na-ionomer. In ASA, polyacrylate rubber particles, grafted with styrene acrylonitrile are dispersed within the polystyrene acrylonitrile (PSAN) matrix surface.[16] Both the blend system shows characteristics transformation of molecular chain conformation when the ionomer content is 30% or above. Below this critical level, the ionomer chains are lying on PSAN matrix surface[21,23] and "mushroom" type morphology was observed. After the critical content of ionomer, both the ASA/Na-ionomer and the ASA/Zn-ionomer blends transformed into "brush" type morphology, where ionomer chains formed "standing" type superstructures. The dynamic rheological measurement of both the blend systems also established this type of molecular chain conformation switchover,[22,24] which was also observed by the SEM and AFM images.[21] The mushroom and brush conformation were explained by two and three humps, respectively, in the loss modulus curves. In addition, in the brush regime, ionic groups of ionomer formed ionic aggregates. This type of ASA/ionomer blend structure was pictured in the form cartoon representation.[22,24] The switchover transformation of these blend systems can be used to make smart polymers if these blends are formulated with specific types of fillers like carbon nanotubes (CNTs), graphite, ferrite, etc.

If the nanotubes are perfectly dispersed in a matrix polymer, a high percolation threshold is observed for electrical conductivity. Nonuniform micro-scale dispersion of carbon nanotubes is one of the key factors to obtain a low percolation threshold value, although some bundling of the nanotubes is involved during the process.[25] In a two-phase polymer system, by controlling the shape of the two phases, nonuniform micro-scale dispersion of carbon nanotubes can be achieved; leading to low percolation thresholds.[25] Our earlier research publications[21,22] show base polymer matrix (50/50 ASA/Na-ionomer blend) formed brush structure, which was experimentally verified by van Gurp–Palmen plot.[21]

Carbon nanotubes having high aspect ratio ($l/d >> 1$) induced percolation threshold at low concentration than spherical ones.[26] The reported percolation threshold limit of carbon nanotubes varies from less than 1% to over 10% in weight.[27] Coleman *et al.*[28] observed up to 10 times more electric conductivity for 8 wt % nanotubes loaded poly(*p*-phenlyenevinylene-co-2,5-dioctoxy-*m*-phenylene vinylene) nanocomposite. Whereas a low SWCNT loaded (0.1% by volume) polyimide /SWCNT nanocomposite films showed a significant 10-fold increment in electrical conductivity without significantly sacrificing optical transmission.[29] Abu-Surrahn *et al.*[30] observed AC conductivity was increased by 500 times when aspect ratio of MWCNT was changed from 30 to 660. Both covalent and noncovalent functionalizations of CNT surface improve CNT dispersion in the matrix; mechanical properties get enhanced but prevent conductivity increase. Costa *et al.*[31] observed this effect on triblock copolymer styrene-butadiene-styrene containing up to 8 wt % carbon nanotubes, which were covalent and noncovalently functionalized.

Our aim at the recent work was to prepare a suitable protective layer polymeric formulation for telecommunication components used in outdoor applications. We exploited the outstanding electrical conduction and thermal stability of CNTs in ASA/Na-ionomer/MWCNT nanocomposite system. Multiwalled carbon nanotubes (MWCNT) were preferred as filler system over single-walled carbon nanotubes (SWCNT) because of lower cost of the former. The matrix system used here is 50/50 by weight of ASA/Na-ionomer blend, as the brush conformation is expected to form percolation threshold at low MWCNT content, and in addition, this blend system has advantages like better thermal stability and heat-sealability.[21] The present article covers the mechanical properties, rheological characteristics (both linear and nonlinear behavior), and electrical properties of the nanocomposites.

EXPERIMENTAL

Materials

Acrylonitrile styrene acrylate (ASA), Luran S 777, was supplied by BASF and it has density of 1.07 g/cm^3, and melt volume rate of 13 g/10 min at 220°C/10 kg load. DuPont, India supplied the Na-ionomer, Surlyn 1601-2, which is a copolymer of ethylene and methacrylic acid (10 mole percent), and the methacrylic acid is 53% neutralized by Na-salt.[32] Surlyn 1601-2 was characterized by its density of 0.94 g/cm^3, melt flow rate of 1.3 g/10 min at 190°C/2.16 kg load, and a DSC melting point of 96.1°C.[22] The multiwalled carbon nanotubes (MWCNTs), produced by catalytic chemical vapor deposition (CVD) method, was procured from Sigma Aldrich (India). It had the diameter of 6–9 nm, 5 μm in length, and amorphous carbon content was <5%.[33]

Nanocomposite Processing

For the nanocomposite preparation, we used melt processing technique that has various advantages like higher throughput, simple process, and more notably, this process is free from contaminants and solvents. In addition, this process can produce high nanotubes loaded (>10%) nanocomposites, which can have Young's modulus up to 200% more than the matrix.[34]

All the ingredients were preconditioned in a vacuum oven at 80°C for at least 48 h under vacuum to eliminate any moisture present within the sample. The dried materials were mixed in right proportions and fed to previously heated twin screw micro-compounder (Haake Mini Lab II, Thermo scientific, Germany). The micro-compounder has two intermeshing, conical, co-rotating screws, which has diameter 5/14 mm (conical), and length 109.5 mm. The processing was performed at 150 RPM screw speed and the barrel temperature was maintained at 250°C. For better and uniform dispersion, online recycling mode was selected, and recycling time was 10 min. The samples were designated as NCNT followed by numerals, which represent the weight percentage of MWCNT.

We used the formula, $V_f = \rho(w_f/\rho_c)$ to calculate the volume fraction (V_f) of MWCNTs, wherever it was necessary. Here, ρ represents the apparent density of the nanocomposite V_f and w_f stand for the volume and weight fraction of MWCNTs in nanocomposites, respectively. The true density (ρ_c) of MWCNT was taken as 2.1 g/cm^3.

Preparation of Specimens

The microinjection molding machine (Haake MiniJet II, Thermo Scientific, Germany) was fitted to the twin-screw micro-compounder die and the melt at 250°C was taken directly into the micro-injection barrel, which was at 250°C temperature. Six hundred bars injection pressure for 4 s, and 450 bars hold pressure for 3 s were applied to make the tensile specimens (Type-V as per ASTM D638 standard) of all the nanocomposites. Forty degree Celsius was the mould temperature during the sample preparation.

The pellets were produced by extruding the hot melt at room temperature, cooled; cut it to pieces and vacuum dried in a vacuum oven at 80°C for at least 4 days. Compression molded sheets were produced by compression molding machine (Carver Press 4120, USA) at 250°C, using a tonnage of 5 tons for 5 min. For the rheological measurements, we used 25-mm dia disks, which were cut from the sheet. The same 25-mm dia disks were also used to make thin films by the same compression-molding machine under the same processing condition for optical microscopy. The electrical measurement instrument uses 12.7-mm dia disk. Prior testing, both the sides of the specimen were made electrically conducting by providing silver paste coating.

After sample preparation, all the specimens were kept in polyethylene bags and immediately vacuum sealed. The vacuum-sealed bags were stored in a vacuum desiccator for at least 21 days for physical aging. EMAA copolymer-based ionomer undergo physical aging process, and during this stage, secondary crystallites are formed at room temperature.[35–39] The formation of secondary crystallites, which continues for 2 to 3 weeks after molding,[40] increases the modulus over time.

Characterization

AFM Study. Semi-contact mode was used for the AFM analysis in the air on a Solver Pro-47 instrument (NT-MDT, Russia). V-shaped silicon nitride coated silicon cantilevers had the tip radius between 20 and 60 nm.

Transmission Electron Microscopy Study. The transmission electron microscopy (TEM) study was performed in Philips CM200 TEM analyser, which was operated under 200 kV.

Optical Microscopy. Optical microscope was used to observe the dispersibility of MWCNTs. Leica DM LM (Leica, Germany) optical microscope was used to study the dispersion of MWCNT in the nanocomposites. The DFC 320 camera attached on the top of the microscope captured the images.

Tensile Strength Determination. The tensile testing was performed in Instron universal tensile testing machine (Model 3366) and ASTM D638 standard was adopted. The crosshead speed was maintained at 10 mm/min. The average data of at least five specimens along with standard deviation are reported here.

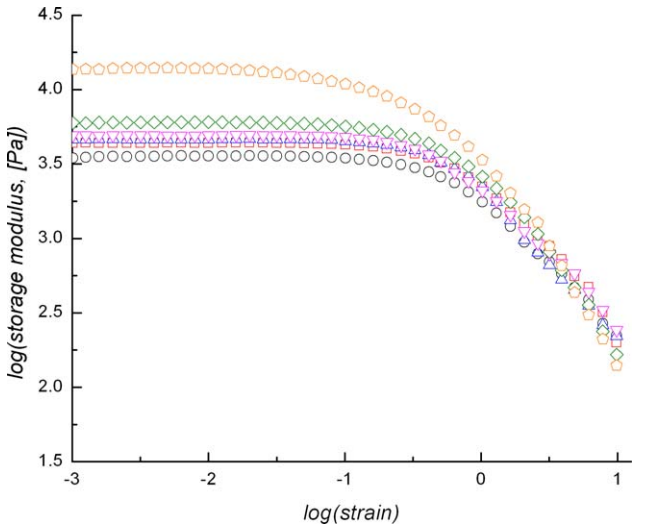

Figure 1. Amplitude sweep for ASA/Na-ionomer/MWCNT nanocomposites. [Color figure can be viewed in the online issue, which is available at wileyonlinelibrary.com.]

Rheological Studies. The linear and the nonlinear rheological properties of the nanocomposites were measured using Bohlin Gemini Rheometer (Malvern Instruments, UK). All the tests were performed between 25 mm diameter parallel-plates apart by 1000 μm distance. The instrument is controlled by Gemini 200 software that generates and analyzes the data. Each experiment was repeated at least thrice for the reproducibility of the measured data. The linear viscoelastic region (LVER) of each nanocomposite system was evaluated by amplitude sweep test. Figure 1 shows the LVER data of all the system. We selected a fixed strain of 0.01% from the linear portion of the LVER curves for the frequency sweep study. The tests were performed from 0.01 to 100 rad/s frequency. The upper plate supply time-dependent strain, $\gamma(t) = \gamma_0 \sin(\omega t)$, to each sample, where γ_0 is the instantaneous strain at zero time ($t = 0$), and ω is the angular frequency. The plate experiences the output as time-dependent shear stress, $\sigma(t) = \sigma_0[G' \sin(\omega t) + G'' cos(\omega t)]$ where, σ_0 is the instantaneous shear stress. G' and G'' denote the storage and loss modulus of the sample, respectively. The isothermal frequency sweep experiments were performed at various temperatures ranging from 200 to 300°C. The Gemini 200 software constructed the master curves at reference temperature (T_{ref}) of 250°C, using the time-temperature superposition principle. For the construction of master curves, we have used the William Landel Ferry (WLF) equation, $\log(a_T) = \frac{-C1(T-T_{ref})}{(C2+T-T_{ref})}$ with $T_{ref} = 250$°C, where a_T is the shift factor (a_T), and both $C1$ and $C2$ are the WLF constants for each nanocomposites system. The relationship $\frac{\eta}{\eta_{ref}} = a_T b_T$ [41] was used for the determination of vertical shift factor (b_T). Here, η and η_{ref} refer the shear viscosities of the nanocomposites at any temperature (T) and at reference temperature ($T_{ref} = 250$°C), respectively. The vertical shift factors (b_T).were determined under viscometry mode, and shear viscosities (not included here) of all the

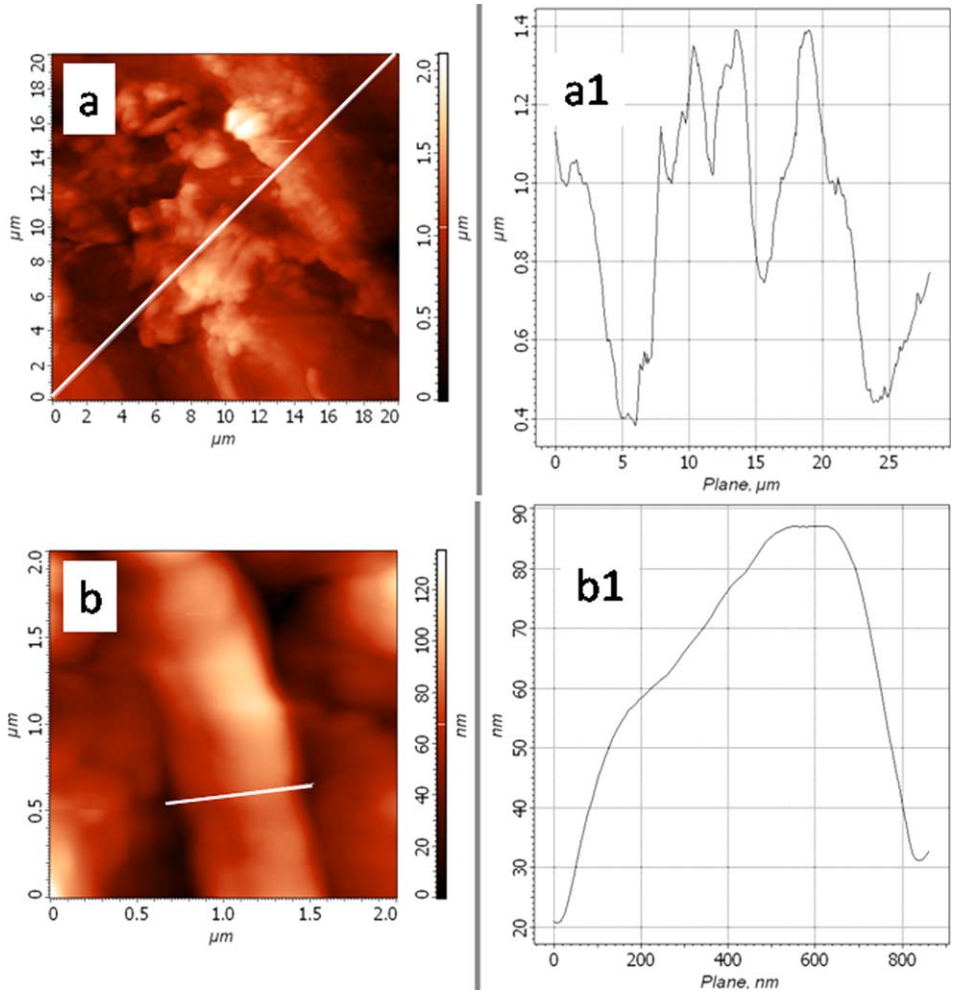

Figure 2. Morphological features of ASA/Na-ionomer/MWCNT nanocomposite systems: (a) AFM image of NCNT 0 showing its brush formation, (a1) topograph of NCNT 0 for marked part, (b) AFM image of NCNT 1.0 showing the formation of network structure, and (b1) topograph of NCNT 1.0 for marked part. [Color figure can be viewed in the online issue, which is available at wileyonlinelibrary.com.]

nanocomposites were estimated over a temperature range of 200–300°C.

The shear viscosities behaviors of the nanocomposites were studied under nonlinear viscoelastic region (Non-LVER). It was evaluated at predefined shear rates of 0.001 to100 s^{-1} and at 250°C temperature. Five parameter Carreau-Yasuda model,[42] as described by eq. (1), was used to examine the dependence of the shear viscosities (η) as a function of shear rate ($\dot{\gamma}$) for all the nanocomposites and the base polymer blend system.

$$\eta = \eta_\infty + (\eta_0 - \eta_\infty)[1+(\lambda\dot{\gamma})^a]^{\frac{(n-1)}{a}} \quad (1)$$

where η, η_0, and η_∞ represent the shear viscosities of the nanocomposite system at any shear rate, at $\dot{\gamma} \rightarrow 0$, and at $\dot{\gamma} \rightarrow \infty$, respectively. λ is called the natural time (the reciprocal of the frequency), where the viscosity of the system changes from the Newtonian region to the non-Newtonian region. The non-Newtonian power index "n" represents the degree of frequency thinning, and has the same value in the power law model. The index parameter "a" controls the transition from the Newtonian to the non-Newtonian region. At low shear rates, when $\dot{\gamma} \ll 1/\lambda$, eq. (1) becomes $\eta = \eta_0$, that is, the material behaves as a Newtonian fluid, whereas at high shear rates ($\dot{\gamma} \gg 1/\lambda$), material follows power-law fluid. The value of n lies in between 0 and 1, the lower value means more deviation from a Newtonian fluid, and for n=1, the Carreau-Yasuda model turns out to be, $\eta = \eta_0$, that is, shear viscosity becomes constant and independent of shear rate (i.e., Newtonian fluid). The Carreau-Yasuda model parameters were determined by the "Solver" tool of Microsoft Excel.

Electric Conductivity Measurement. The AC conductivity was measured with spectrometer (Alpha Tab, Novocontrol Technologies, Germany) on 12.7-mm dia circular specimens having an average thickness of about 1.8 mm. The testing was performed in the frequency ranging from 10^{-3} Hz to 10^7 Hz. Prior testing, both the faces of the samples were coated with silver paste and dried to ensure good surface contact.

Heat Seal Strength Measurement. The effect of MWCNTs on the heat seal behavior of ASA/Na-ionomer/MWCNT nanocomposites on aluminum surfaces was performed by determining

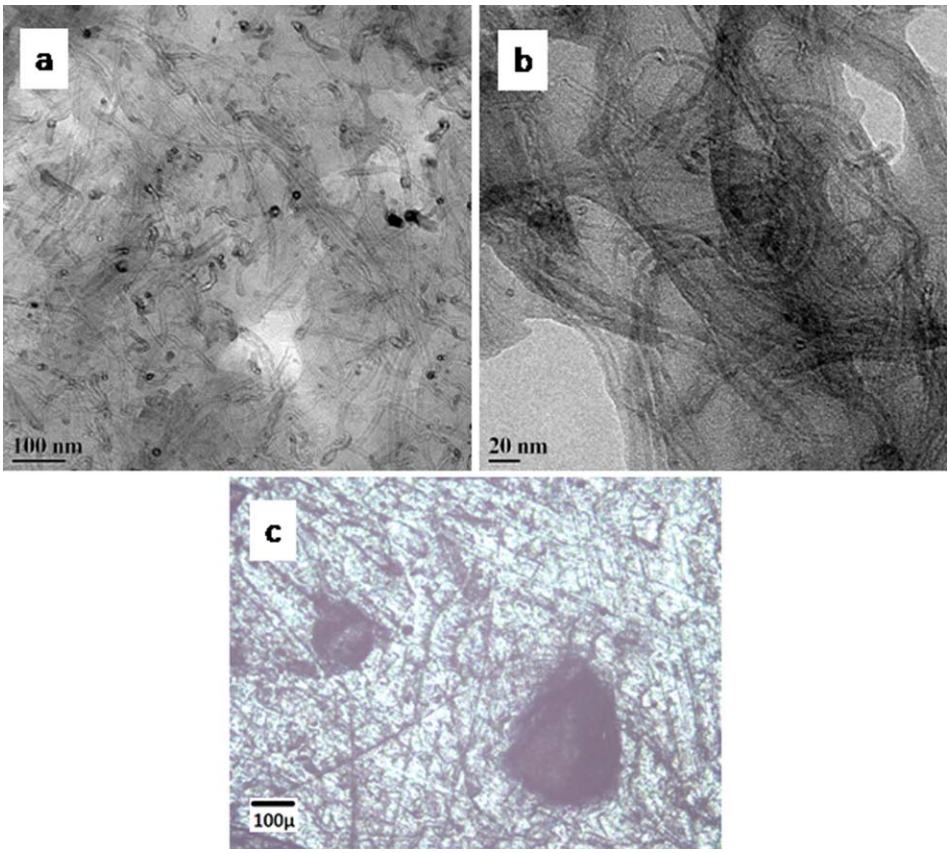

Figure 3. TEM images of NCNT 1.0 at (a) lower magnification, (b) higher magnification, and (c) optical micrograph of NCNT 5.0 showing nanotube aggregates. [Color figure can be viewed in the online issue, which is available at wileyonlinelibrary.com.]

T-peel strength as per ASTM D1876 standard. A temperature of 200°C was selected for the experiment, as this is the plateau initiation temperature (T_{pi}) for ASA/Na-ionomer system.[21] The "T-peel" specimens were prepared by using two L-shaped aluminum strips, which were preheated to 200°C, rectangular shaped nanocomposite sample was placed in between the strips, heat once again at 200°C and pressed for 1 s dwell time. The average thickness of the sealing polymer layer was 0.025 mm. Excess polymer was scrapped off while the specimen was still hot. The specimens were preconditioned in a vacuum desiccator for at least 48 h before testing. The T-peel strength was measured in Instron universal tensile testing machine (Model 3366) using crosshead speed of 254 mm/min.

RESULTS AND DISCUSSION

Morphological Studies

The base polymer blend (50/50 ASA/Na-ionomer) is a biphasic brush polymer system that showed two minima in van Gurp–Palmen plot; a characteristic feature of a typical brush polymer.[21] ASA has core-shell morphology, where butyl acrylate elastomers act as core and poly(styrene acrylonitrile) which are grafted on butyl acrylate elastomer are shell; these core-shell structures are dispersed in poly(styrene acrylonitrile) phase.[43] Upon incorporation of Na-ionomer to ASA above 30%, ionomer content leads to brush formation.[21] Na-ionomer chains containing acrylic acid component are grafted only on butyl acrylate surface because of similar type chemical nature and formed brush structures.[21] Therefore, the brush formations are also dispersed in poly(styrene acrylonitrile) phase of ASA. Figure 2(a) shows the AFM image of base NCNT 0 blend along with topograph [Figure 2(a1)]. The topograph and the AFM image suggest "peaks and valleys" type surface topology for the base NCNT 0 blend. The formation of scattered brush formation leads to peaks that are present in the poly(styrene acrylonitrile) valleys. This type of phase-separated morphology is beneficial for nonuniform micro-scale dispersion of carbon nanotubes[25,44] to form electrical percolation at low nanotube content; nanotubes are generally isolated in one phase either due to favorable interactions with that phase or kinetic factors that limit the crossing over into the other phase.[25] The shape of the phases also induces nonuniform micro-scale nanotube dispersion; nanotubes are deposited at the edges of the polymer chains.[25] These type nonuniform nanotube dispersion was observed in different polymer systems.[25,44] Figure 2(b) represents the AFM image of NCNT 1.0 nanocomposite that shows a tube-like pattern in the surface; this tube-like pattern can be ascribed to formation of nanotube network, which is also observed in TEM image [Figure 3(b)]. The large diameter of the tube-like pattern as shown in the topograph [Figure 2(b1)] suggest re-bundling of nanotubes in our viscous polymer blend along the valleys of the brush polymer blend. The re-bundled nanotubes were positioned at the edges of the brush layers due

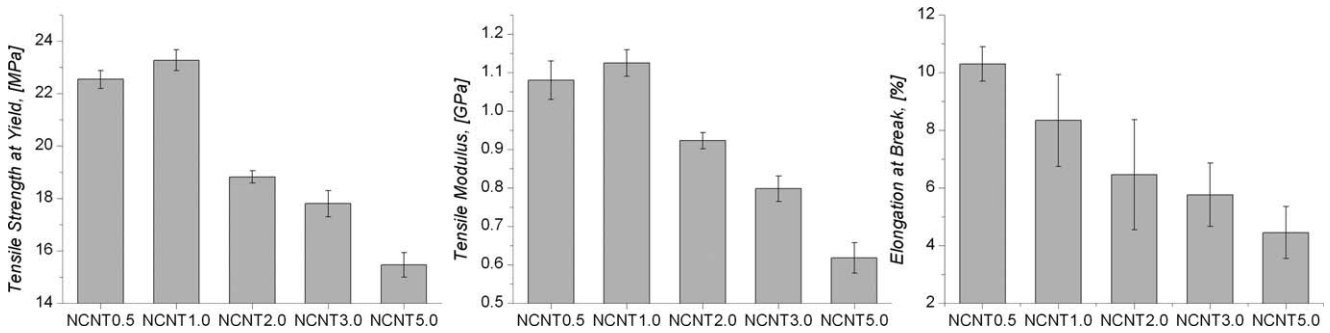

Figure 4. Mechanical properties of the ASA/Na-ionomer/MWCNT nanocomposite systems. The base polymer blend NCNT 0 (50/50 ASA/Na-ionomer blend) had tensile strength at yield of 21.9 MPa, tensile modulus of 0.997 GPa, and elongation at break of 27.24%.[21]

to highly kinetically dependent phenomenon.[25] The peaks and valleys type surface topology thus helps to add the nanotubes preferentially in the valleys.

The lower magnification TEM image of NCNT 1.0 in Figure 3(a) shows some nanotube networks in addition to some scattered nanotubes. These nanotube networks are clearly visible in the higher magnification TEM image in Figure 3(b). Both these TEM images suggest that the nanotubes were also present on the peaks in addition to carbon nanotubes network structure in the valleys. This network formation is also observed in AFM image in Figure 2(b). This type of network distribution of CNTs may be due to the incomplete interdiffusion of the polymer[45,46] and was first detected by Grunlan *et al.*[47]

The higher loading level of nanotubes leads to formation of agglomerates as observed in optical microscopy image in Figure 3(c). This may be due to Van der Walls type of interaction among the nanotubes.

Mechanical Properties

The effect of MWCNT incorporation on the mechanical performance of ASA/Na-ionomer/MWCNT nanocomposites is displayed in Figure 4. MWCNT addition to the blend shows the reinforcement effect in the form of increased tensile modulus (1.08 GPa) and tensile strength (22.54 MPa) as compared with the base polymer blend. The NCNT 0 (50/50 ASA/Na-ionomer blend) had tensile strength at yield of 21.9 MPa, tensile modulus of 0.997 GPa, and elongation at break of 27.24%.[21] The one way to measure the reinforcement effect is to determine the rate of increase in Young's modulus (dY/dV_f) to the volume fraction (V_f) of MWCNT at low nanotubes content[48] are found to be about 57 GPa against theoretical maximum value of 400 GPa.[49] The low values can be attributed to the nonuniform micro-scale dispersion of nanotubes that were deposited preferentially on the valleys of phase separated peaks and valleys type surface topology. This type of nanotube dispersion is the cause of inferior mechanical performance.[25] Another reason for low mechanical properties may be due to decrease in the average length of MWCNTs when nanocomposite is produced in miniature twin-screw melt-mixers,[50] that we have used in making of the nanocomposites. As per literature, the average length of MWCNTs was found to decrease by 33% irrespective of the details of the mixers.[50] However, the mechanical performances can be further improved by covalently surface functionalization of carbon nanotubes that can efficiently transfer interfacial stress–strain between the nanotubes and the polymer matrix.[51] Two factors control the mechanical strength of MWCNT composites. Good interfacial adhesion between the polymer matrix and nanoparticles efficiently transfer the load and thereby increase the mechanical properties. The poor interfacial adhesion makes the MWCNTs to behave like holes or nanostructure flaws. They act as local stress concentrations centers and accelerate the mechanical failure.[50] The other factor is the level of nanotubes dispersion and their mode of dispersion. The load is effectively distributed if the nanotubes are well dispersed in the matrix. On the other hand, the poor dispersion of the nanotubes results in the failure by bundle separation, instead of MWCNT failure itself.[51–53] The considerable improvement in both tensile modulus and tensile strength at low MWCNT content (up to 1%) is due to the enhanced ASA/Zn-ionomer/MWCNT interactions. At 1% MWCNT content, network formations [Figure 3(b)] of MWCNTs are observed. Further addition of MWCNT form agglomerates [Figure 3(c)]. Both the agglomerates and the nonuniform micro-scale distributions of networks reduce both the tensile strengths and the tensile moduli. However, MWCNTs increase the deformability of the rigid interface between MWCNTs and ASA/Na-ionomer matrix and are responsible for the decreasing trend in elongation at break.

Rheological Properties

Linear Rheological Properties. The van Gurp–Palmen plot (vGP plot),[54] where the phase angle (δ) is plotted as a function of absolute value of the complex modulus |G*|, is sensitive to the molecular weight, molecular weight distribution, and molecular architectures of the polymers.[55] The base polymer blend (NCNT 0, which is a 50/50 blend of ASA and Na-ionomer) has brush morphology and shows two characteristic minima in vGP plot.[21] The first minimum at higher modulus represents the relaxation of the side chains and the second minimum at lower modulus around 2–5 kPa relates to the backbone relaxation of the whole brush polymer.[56] Here, instead of complex modulus that include the storage and loss modulus components, the phase angle (δ) is plotted against storage modulus (Figure 5). This plot will help to correlate the effect of addition of nanotubes on the side chains (here "Arm") and backbone chains mechanical performance. Figure 5 shows that up to 1% nanotube content, the first minima that correspond to Arm here shows at lower storage modulus compared with base polymer

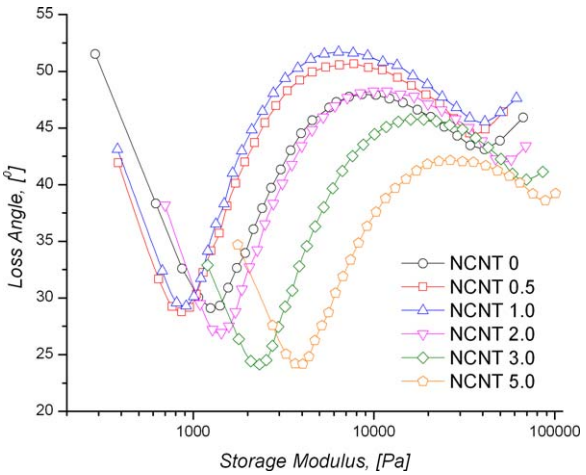

Figure 5. van Gurp–Palmen plot of the ASA/Na-ionomer/MWCNT nanocomposite systems. [Color figure can be viewed in the online issue, which is available at wileyonlinelibrary.com.]

blend (NCNT 0); thereafter, this minimum is shifted to higher storage modulus. The lower storage modulus of the Arm up to 1% nanotube content can be attributed to the increased separation between the Arms as a consequence of low level nanotube addition. Above 1% nanotube content, the shifting of the first minimum at higher storage modulus indicates the closeness of the side chains. Similar observation is noticed for the second minimum that is related to backbone chains at valley.

The linear rheological relaxation spectra, which provides the information about the topological structure of polymers is shown in Figure 6. The higher storage modulus (G') compared with loss modulus (G'') for all the nanocomposite systems indicate the unentangled polymer behavior.[57] The loss modulus spectrums also represent the fingerprint of the chain topology. The cartoon representation[22] of the base 50/50 ASA/Na-ionomer blend predicts three tiers "Caylay Tree" type network[58] and the characteristic three humps were observed in the loss modulus relaxation spectra. As per the proposed structure,[22] the backbone consists of butyl acrylate rubber chains of ASA polymer and the Zn-ionomer chains are the arms. The arms have two parts—the part, which connects the backbone and the ionic cross-links is designated as "Arm II." The rest portion, which starts from ionic cross-links to the free end of the Na-ionomer chain, has been represented by "Arm I." When MWCNTs are added, the nanoparticles are expected to deposit in between the Arm I polymer chains, and around the backbone chains and valleys consisting of PSAN matrix. MWCNTs are also expected to entrap in between the "Arm II" chains. This phenomenon is represented in Figure 7.

For architecturally complex macromolecules like ASA/Na-ionomer/MWCNT nanocomposite system, we have used the hierarchical rule[59] to explain the relaxation spectrum, shown in Figure 6. As per this rule, the relaxation modulus spectrum of a branched polymer has three major contributions—high-frequency relaxation, arm relaxation, and backbone relaxations. The rule states that high frequency relaxation occurs first at higher frequencies, arm or branch relaxation follows next, and backbone relaxation takes place last at lower frequencies. Figure 6 also shows the $\tan\delta$ spectra, the ratio of loss modulus ($G''(\omega)$) to storage modulus ($G'(\omega)$), that provides more sensitive data in the relaxation process. The minima in $\tan\delta$ spectra represents the onset time of a new relaxation process of the polymer chain. The relaxation times [$\tau = 1/(a_T\omega)$] of the polymer chains of our nanocomposite system are summarized in Table I. The high frequency relaxation time ($\tau_{High\ Freq.}$) represents the time taken by the free dangling Arm I under high frequency. It is the fastest relaxation time and represents the onset of Arm I relaxation. Similarly, Arm I relaxation time ($\tau_{Arm\ I}$) and Arm I relaxation time ($\tau_{Arm\ II}$) of all the nanocomposite systems represent the time required to relax by respective Arm I and Arm II.

The relaxation process starts from Arm I. Under high frequencies, this free dangling arm (Arm I) of Na-ionomer relaxes by local Rouse-like transitional motions and longitudinal segmental motions,[60] but does not encounter any tube constraint, which was proposed by Doi and Edwards[61] in the tube theory. At the end of high frequency relaxation process, the free dangling Arm I reorient by the applied strain and the characteristic $\tan\delta$ minimum is observed. Table I shows that the incorporation of MWCNT up to 1% content increases $\tau_{High\ Freq.}$ relaxation time and further increase in MWCNT content reduces the $\tau_{High\ Freq.}$ relaxation time. Two opposing effects are observed during the relaxation of Arm I. The TEM image in Figure 3(a) shows that nanotubes are present on the peaks comprising the Arm layers in addition to nanotube networks that are formed in the valleys. The initial addition of MWCNT (at low nanotube content) may have increased the separation between Arm I; this effect can also be verified by lower minima values of storage modulus in van Gurp–Palmen plot for NCNT 0.5 and NCNT 1.0 (Figure 5). The maximum separation may have happened around 1% MWCNT content. Further MWCNTs addition may not accommodate them around Arm I. On the other hand, the interaction between Arm I and MWCNTs impede the relaxation process and this is perhaps the dominating factor above 1% MWCNT content. The nanotube addition also increases the polymer chain separation; higher polymer chain interaction can also retard the relaxation process. The rest part of the polymer chains are remained in virtually frozen condition due to the large friction in the brush arms (Arm II) at the grafting points.[62]

The Arm I relaxes in similar fashion and the effect of MWCNT remains the same on their relaxation time ($\tau_{Arm\ I}$). The shorter Arm I branches take less time to relax as compared with longer branches, and consequently, the shorter branch relaxation takes place at higher frequency ($\tau = 1/\omega = 1/2\pi f$).

Arm II relaxation is followed by Arm I relaxation. At this stage, both the storage modulus ($G'(\omega)$) and loss modulus ($G''(\omega)$) decrease in similar fashion. The average slope of both $G'(\omega)$ and $G''(\omega)$ represent the power-law exponents, which are approximately equal to 0.5 and suggest Rouse-like chain dynamics for Arm II. Similar observation is observed for carefully controlled comb polymers[63] and un-entangled polyelectrolytes.[64] Because Arm II chains are attached in between the grafting

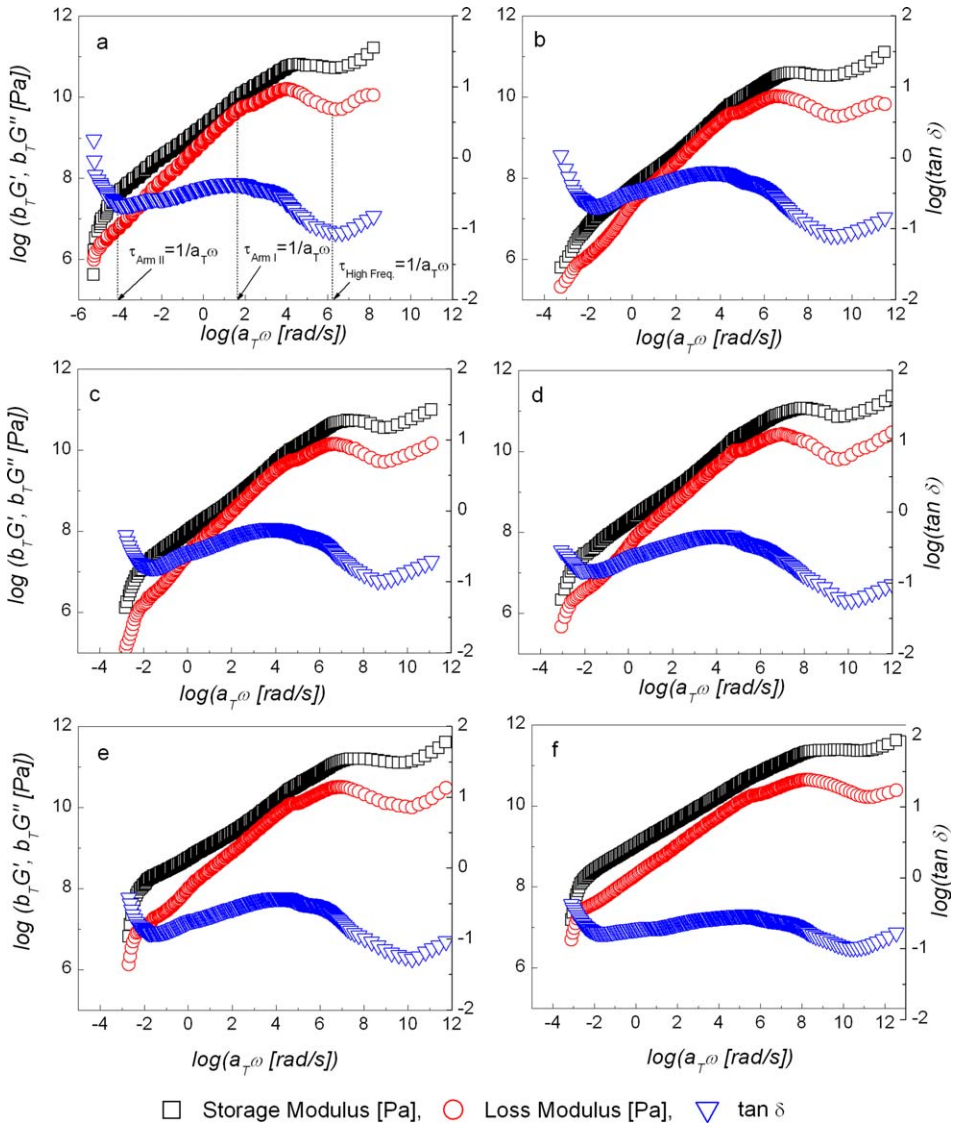

Figure 6. Dynamic moduli and tangent of phase lag tan δ for (a) NCNT 0, (b) NCNT 0.5, (c) NCNT 1.0, (d) NCNT 2.0, (e) NCNT 3.0, and (f) NCNT 5.0 nanocomposite systems $T_{ref} = 250°C$. [Color figure can be viewed in the online issue, which is available at wileyonlinelibrary.com.]

points on backbone and the ionic crosslink, its relaxation by the reptation process are not possible.[62] The completion of Arm II relaxation shows another tan δ minimum, and the corresponding relaxation time ($\tau_{Arm\ II}$) by Arm II is the longest relaxation time. The incorporation of MWCNTs lowers the relaxation time continuously. This can be explained if we look into the cartoon representation shown in Figure 7. The incorporation of MWCNT around the Arm II has little effect on increasing the spaces around them, as both the ends of Arm II are connected, but impede the relaxation process.

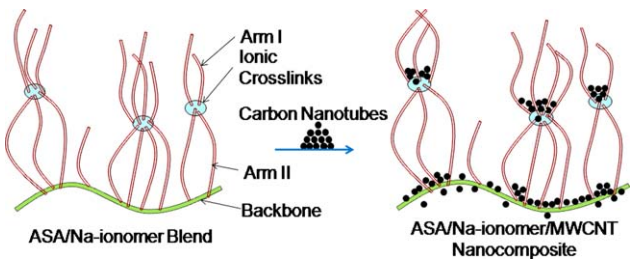

Figure 7. Cartoon representation ASA/Na-ionomer/MWCNT nanocomposite system. [Color figure can be viewed in the online issue, which is available at wileyonlinelibrary.com.]

The backbone relaxation is observed by another hump in loss modulus (G″) spectra at lower frequencies. There are two methods for backbone relaxation—the reptation process and the contour length fluctuation (CLF) process. The process, which generates lower relaxation time, is the preferred one.[65] During CLF process, the grafting points and MWCNTs around the backbone act as friction points and thereby enhance the relaxation time. If the relaxation time is more than the reptation process, the backbones relax *via* reptation process.

Nonlinear Rheological Properties. It is essential to study the processing behavior of newly developed system. Figure 8 shows

Table I. Linear Viscoelastic Properties of ASA/Na-Ionomer/MWCNT Nanocomposite Systems

Material	C1	C2, [^{0}K]	Average Slope of G' for Arm II	Average Slope of $G''$for Arm II	$\tau_{Arm\,II}$, [s]	$\tau_{Arm\,I}$, [10^{-3} s]	$\tau_{High\ Freq.}$, [10^{-9} s]
NCNT 0	2.29	220.14	0.45	0.49	327.87	6.309	434.01
NCNT 0.5	2.32	224.96	0.47	0.53	286.42	7.642	879.02
NCNT 1.0	1.45	225.93	0.49	0.45	263.03	8.629	1786.49
NCNT 2.0	0.93	226.54	0.47	0.47	141.22	0.018	0.144
NCNT 3.0	0.81	224.87	0.46	0.46	52.65	0.01	0.066
NCNT 5.0	0.76	227.73	0.45	0.45	46.24	0.002	0.033

the effect of MWCNT on steady shear viscosity of ASA/Na-ionomer/MWCNT nanocomposites under shear rates. There are two characteristic regions in the shear curves. The first region comprises typical Newtonian region at low shear rates, and the second one is the non-Newtonian shear-thinning region at high shear rates. In the Newtonian regime, at any fixed shear rate, the viscosity increases with increase in MWCNT content. The significantly higher viscosity shear viscosity above 1% MWCNT content may be attributed to the formation of agglomerates, which hinder the flowability of the polymeric chains. In the non-Newtonian region, the viscosity decreases monotonically as the shear rate is increased. An interesting feature of lower shear viscosity is observed for NCNT 3.0 and NCNT 5.0 over the base polymer blend at higher shear rates. This more shear thinning action of highly MWCNT-loaded samples is due to the formation of flocculation and agglomeration of MWCNTs that under high shear rates orients themselves in the flow direction and the nanoparticles slide over each other[66] and thus enhances the flowability.

To compare the viscosity data more efficiently, the viscosity data were analyzed by using Carreau-Yasuda model eq. (1). The model parameters of each batch are summarized in Table II. The low RMS deviation suggests good model fitting. The zero-shear-viscosity (η_0) of nanocomposites increases steadily with an increase in MWCNT content and noteworthy increase is observed for NCNT 5.0. The agglomerates of MWCNTs in NCNT 5.0 may be responsible for high zero-shear-viscosity (η_0). Table II shows that the infinite-shear-viscosities (η_∞) of nanocomposites come close to low and almost constant value. Under high shear rates, the flow drag orients all the MWCNTs in the flow direction and reduces the MWCNT/polymer interaction substantially. Therefore, at high shear rates, the base ASA/Na-ionomer dominates the shear viscosity of the nanocomposite[67] and the infinite-shear-viscosity (η_∞) is independent of MWCNT content. The natural time constant (λ), which represents the time when the viscosity changes from Newtonian to non-Newtonian region, initially increases up to 2% MWCNT content, and thereafter a decreasing trend is observed with further increase in MWCNT content. The polymer/MWCNT interaction at lower MWCNT level inhibits the flowability and thus delays the Newtonian/non-Newtonian transition. However, at higher nanotubes content, MWCNT/MWCNT interaction predominates over polymer/MWCNT interaction and nanotubes/nanotubes slippage induce the shear thinning behavior at the earlier stage. The same justification is applicable to the trends observed for non-Newtonian power law index (n) and parameter "a."

Electrical Properties

The effect of sinusoidal frequencies (ω) on the AC electrical conductivity of the ASA/Na-ionomer/MWCNT nanocomposites is represented in double logarithmic scales and shown in Figure 9. There are two regions—the first region is the frequency-independent plateau region, which is followed by frequency-dependent conductivity that increases with an increase in frequency. Such type of conductivity (σ_{AC}) can be better represented by Power-law equation eq. (2).

$$\sigma_{AC} = \sigma_{DC} + A\omega^n, \qquad 0 < n < 1 \tag{2}$$

where the temperature-dependent parameter "A" is a constant, and the frequency exponent "n" depends on both frequency and temperature.[68] The DC conductivity (σ_{DC}) is measured from the plateau of the graph. The AC conductivity rises after a critical frequency (ω_c) and conductivity dispersion is noticed. With an increase in MWCNT concentration, the critical frequency (ω_c) has been moved toward higher frequency. The formation of high degree MWCNT "network-like" structures may

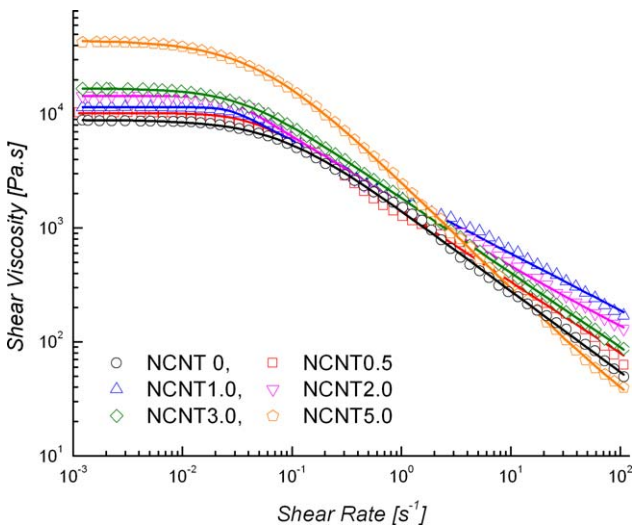

Figure 8. Shear viscosity as a function of ASA/ Na-ionomer/MWCNT nanocomposite systems. The solid lines represent the model fitting data. [Color figure can be viewed in the online issue, which is available at wileyonlinelibrary.com.]

Table II. Rheological Parameters Obtained by the Carreau-Yasuda Model for ASA/Na-Ionomer Blend and its Nanocomposites

Material	η_0, [Pa.s]	η_∞, [Pa.s]	λ, [s]	a	n	RMS deviation
NCNT 0	8866	3.0	12.9	1.2	0.29	0.039
NCNT 0.5	10195	2.7	23.3	2.2	0.37	0.070
NCNT 1.0	11470	2.9	38.2	5.2	0.50	0.059
NCNT 2.0	14324	3.2	37.9	5.2	0.42	0.058
NCNT 3.0	16746	3.7	28.7	1.5	0.34	0.016
NCNT 5.0	44223	4.1	20.6	1.1	0.06	0.025

be responsible for this behavior.[69] The brush morphology as depicted in Figure 7 and the peaks and valleys type surface topology helped the nanotubes to deposit on the valleys; thus, by controlling the shape of the two phases, nonuniform microscale dispersion of carbon nanotubes are achieved.[25]

We have determined the percolation threshold (p_c) from the DC conductivity (σ_{DC}) data. The classical percolation theory, described in eq. (3), has been used for this purpose. The equation is valid, when $p > p_c$and $(p- p_c)$ is small.

$$\sigma_{DC} = \sigma_{DC,0}(p-p_c)^t \quad (3)$$

Where, $\sigma_{DC,0}$ and exponent "t" are constant for a particular system. When the MWCNTs fraction (p) is beyond the percolation threshold (p_c), a sharp increase in the conductivity is observed because of the formation of conductive paths. One important parameter of eq. (3) is the conductivity exponent "t" that reflects the type of MWCNT network dimension of the system. For two-dimensional (2D) network, the value of t is in the range of 1.1–1.3, and for three-dimensional (3D) network system, t becomes 1.6–2.[70,71] The effect of MWCNT content on DC conductivity along with the model eq. (3) fitted data is shown in Figure 10. The value of percolation threshold (p_c) and the exponent t for ASA/Na-ionomer/MWCNT nanocomposites are found to be 1.00 and 1.3, respectively. The value of t suggests the formation of 2D network system for ASA/Na-ionomer/MWCNT nanocomposites. After the percolation threshold, there is about 8 orders of magnitude increase in DC conductivity as compared with the base polymer blend.

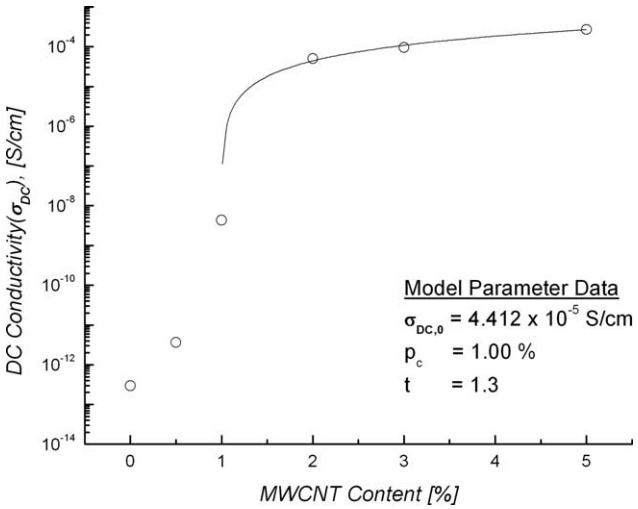

Figure 10. Effect of MWCNT on DC electrical conductivity for ASA/Na-ionomer/MWCNT nanocomposites. The solid line represents the model data.

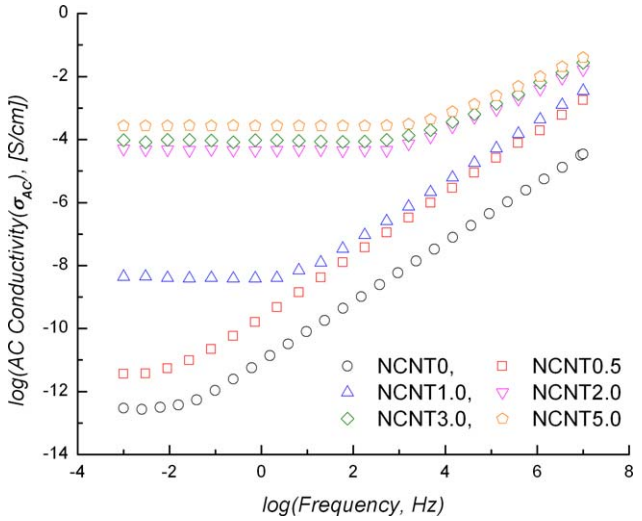

Figure 9. Variation of AC electrical conductivity as a function of frequency for ASA/Na-ionomer/MWCNT nanocomposites. [Color figure can be viewed in the online issue, which is available at wileyonlinelibrary.com.]

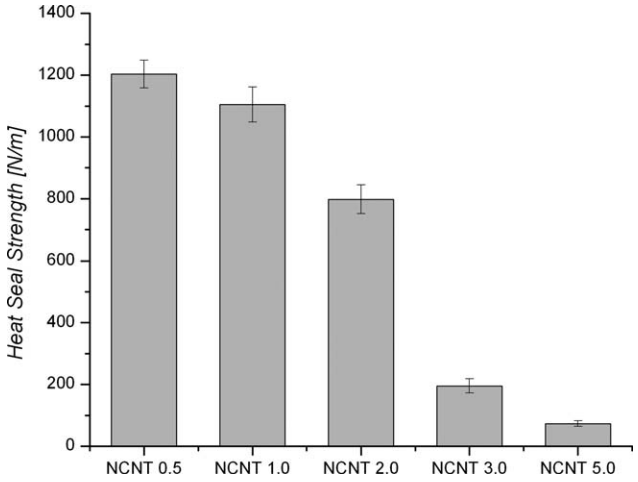

Figure 11. Heat seal behavior of ASA/ Na-ionomer/MWCNT nanocomposite.

Seal Strength

Figure 11 shows the effect of MWCNT content on the heat seal behavior of ASA/Na-ionomer/MWCNT nanocomposites. The base polymer blend (50/50 ASA/Na-ionomer blend) has 1245 N/m heat seal strength.[21] The MWCNT incorporation reduces the T-peel strength of the nanocomposites, and the major reduction of the strength is observed after 1% MWCNT contents. Therefore, MWCNT content is responsible for the lowering of the heat seal behavior and the drastic fall at higher nanotubes content is due to the formation of agglomerates.

CONCLUSION

The effects of MWCNT on 50/50 ASA/Na-ionomer blend were characterized for its mechanical, rheological, and electrical properties. MWCNTs provided reinforcement effect at lower MWCNT content and showed moderate (dY/dV_f) value. However, above 1% MWCNT content, both the tensile modulus and yield strength were decreased because of poor dispersion and formation of agglomerates by MWCNTs.

MWCNTs also affected the molecular chain dynamics of our nanocomposite system. The high frequency relaxation time and the Arm I relaxation time are increased up to 1% MWCNT content and thereafter a decreasing trend is observed. The initial addition of nanoparticles around Arm I increased its free volume, which allowed them to relax slowly. The nanoparticles/Arm I interaction predominated at higher loading of MWCNTs and relaxation process became faster. However, MWCNTs acted differently with Arm II relaxation process. As both the ends of Arm II are connected (Figure 5), the nanoparticles are not able to increase the spaces around Arm II effectively, but the MWCNT/Arm II interaction impedes the relaxation process. Thus, with increase in MWCNTs incorporation lowered the relaxation time of Arm II continuously.

ASA/Na-ionomer/MWCNT nanocomposite system showed typical Newtonian region followed by non-Newtonian shear thinning region in the viscosity graph. The Carreau-Yasuda model eq. (1) is found fit for our system. The nanoparticles aggregates increased the zero shear viscosity of NCNT 5.0 largely. However, at high shear rates, the flow drag oriented the nanoparticles in the flow direction and thus lowered the polymer/MWCNT interaction extensively. The nanotubes/nanotubes slippage enhances the flowability and thus high MWCNT content samples, like NCNT 3.0 and NCNT 5.0 showed lower shear viscosities at high shear rates. Similarly, at high shear rates, polymer/MWCNT interaction becomes negligible and the system viscosity governs by the matrix itself. Consequently, all the system showed almost same infinite shear viscosity (η_∞). At lower MWCNT content, polymer/MWCNT interaction controls the system viscosity, but at higher MWCNT loading, nanotubes/nanotubes interaction predominates. For this reason, the natural time constant (λ), the non-Newtonian power law index (n) and parameter "a" increased up to 1% MWCNT content and thereafter, they showed the decreasing trend.

Based on the classical percolation theory, the DC conductivity data show that the percolation was reached at 1% MWCNT content by weight. The low percolation threshold value may be due to the peak and valley type surface topology [Figure 2(a)] of the base polymer blend. Above the percolation limit, there are formations of 2D networks of MWCNTs and that has also been verified by the TEM image [Figure 3(a,b)]. After reaching percolation, there is 8 orders of magnitude increment of the AC conductivity for NCNT 2.0.

ACKNOWLEDGMENTS

The authors duly acknowledge the Sophisticated Analytical Instrumental Facility (SAIF), IIT Bombay for TEM analysis.

REFERENCES

1. Ijjima, S. *Nature* **1991**, *354*, 56.
2. Rinzler, A. G.; Hafner, J. H.; Nikolaev, P.; Lou, L.; Kim, S. G.; Tomanek, D.; Nordander, P.; Cobert, D. T.; Smalley, R. E. *Science* **1995**, *269*, 1550.
3. de Heer, W. A.; Chatelain, A.; Ugarte, D. *Science* **1995**, *270*, 1179.
4. Collins, P. G.; Zettl, A.; Bando, H.; Thess, A.; Smalley, R. E. *Science* **1997**, *278*, 100.
5. Du, J.-H.; Bai, J.; Cheng, H.-M. *Express Polym. Lett.* **2007**, *1*, 253.
6. Bauhofer, W.; Kovacs, J. Z. *Compos. Sci. Technol.* **2009**, *69*, 1486.
7. Al-Saleh, M. H.; Sundararaj, U. *Carbon* **2009**, *47*, 2.
8. Holiday, L. *J. Polym. Sci. Polym. Lett. Ed.* **1976**, *14*, 114.
9. Bazuin, C. G.; Eisenberg, A. *Ind. Eng. Chem. Prod. Res. Dev.* **1981**, *20*, 271.
10. MacKnight, W. J.; Earnest, T. R. *J. Polym. Sci. Part D Macromol. Rev.* **1981**, *16*, 41.
11. Peiffer, D. G.; Hager, B. L.; Weiss, R. A.; Agarwal, P. K.; Lundberg, R. D. *J. Polym. Sci. Polym. Phys. Ed.* **1985**, *23*, 1869.
12. Longworth, R. In Thermoplastic Ionic Polymers, Ionomers. Holiday, L., Ed.; Ionic Polymers, Ionomers. Wiley: New York, **1975**; p 69.
13. Wu, S.; Guo, Q.; Kraska, M.; Stuhn, B.; Mai, Y. W. *Macromolecules* **2013**, *46*, 8190.
14. Dolog, R.; Weiss, R. A. *Macromolecules* **2013**, *46*, 7845.
15. Grande, A. M.; Castelnovo, L.; Landro, L. D.; Giacomuzzo, C.; Francesconi, A.; Rahman, M. A. *J. Appl. Polym. Sci.* **2013**, *130*, 1949.
16. McKee, G. E.; Kistenmacher, A.; Goerrissen, H.; Breulmann, M. In Modern Styrenic Polymers, Polystyrenes Styrenic Copolymers. Scheirs, J., Priddy, D. B., Eds.; Wiley: West Sussex, **2002**; Chapter 16, p 341.
17. Kamg, E. A.; Kim, J. H.; Oh, S. Y.; Rhee, W. *Polym. Eng. Sci.* **2000**, *40*, 2374.
18. Kim, W. N.; Burns, C. M. *Polym. Eng. Sci.* **1988**, *28*, 1115.
19. Liu, Z.; Deng, Y.; Han, Y.; Chen, M.; Sun, S.; Cao, C.; Zhou, C.; Zhang, H. *Ind. Eng. Chem. Res.* **2012**, *51*, 9235.
20. Seo, Y. S.; Kim, J. H.; Kim, C. K.; Lee, R.; Keum, J. K. *J. Appl. Polym. Sci.* **2005**, *96*, 2097.

21. Datta, P.; Guha, C.; Sarkhel, G. *Polym. Eng. Sci.* **2014**; DOI: 10.1002/pen.23998.
22. Datta, P.; Guha, C.; Sarkhel, G. *Polym. Adv. Technol.* **2014**, *25*, 1454.
23. Datta, P.; Guha, C.; Sarkhel, G. *Polym. Plast. Technol. Eng.* **2014**, *53*, 80.
24. Datta, P.; Guha, C.; Sarkhel, G. *J. Macromol. Sci. Part A Pure Appl. Chem.* **2014**, *51*, 820.
25. Grady, B. P. *Macromol. Rapid Commun.* **2010**, *31*, 247.
26. Martin, C. A.; Sandler, J. K.; Shaffer, M. S.; Schwarz, M. K.; Bauhofer, W.; Schulte, K.; Windle, A. H. *Compos. Sci. Technol.* **2004**, *64*, 2309.
27. Sandler, J. K.; Kirk, J. E.; Kinloch, I. A.; Shaffer, M. S.; Windle, A. H. *Polymer* **2003**, *44*, 5893.
28. Coleman, J.; Curran, S.; Dalton, A.; Davey, A.; McCarthy, B.; Blau, W.; Barklie, R. C. *Phys. Rev. B* **1998**, *58*, R7492.
29. Park, C.; Ounaies, Z.; Watson, K.; Crooks, R.; Smith, J., Jr.; Lowther, S.; Connell, J. W.; Siochi, E. J.; Harrison, J. S.; St. Clair, T. L. *Chem. Phys. Lett.* **2002**, *364*, 303.
30. Abu-Surrahn, A. S.; Al-Ramahi, E.; Jawad, S. A.; Hallak, A. B.; Khattari, Z. *Phys. B Condens. Matter* **2015**, *463*, 76.
31. Costa, P.; Silva, J.; Ansón-Casaos, A.; Martinez, M. T.; Abad, M. J.; Viana, J.; Lanceros-Mendez, S. *Compos. Part B* **2014**, *61*, 136.
32. Suh, K. S.; Damon, D.; Tanaka, J. *IEEE Trans. Dielectr. Electr. Insul.* **1985**, *2*, 1.
33. Sigma-Aldrich Product; Available at: www.sigmaaldrich.com/catalog/product/aldrich/724769?lang=en&region=IN, accessed on October 17, 2014.
34. Liu, T. X.; Phang, I. Y.; Shen, L.; Chow, S. Y.; Zhang, W.-D. *Macromolecules* **2004**, *37*, 7214.
35. Marx, C. L.; Cooper, S. L. *J. Macromol. Sci. Part B* **1974**, *9*, 19.
36. Tsujita, Y.; Shibayama, K.; Takizawa, A.; Kinoshita, T.; Uematsu, T. *Int. J. Appl. Polym. Sci.* **1987**, *33*, 1307.
37. Kohzaki, M.; Tsujita, Y.; Takizawa, A.; Kinoshita, T. *J. Appl. Polym. Sci.* **1987**, *33*, 2393.
38. Kuwabara, K.; Horii, F. *J. Polym. Sci. Part B Polym. Phys.* **2002**, *40*, 1142.
39. Kulkarni, H. P.; Mogilevsky, G.; Mullins, W. M.; Wu, Y. *J. Mater. Res.* **2009**, *24*, 1087.
40. Spencer, M. W.; Wetzel, M. D.; Troeltzsch, C.; Paul, D. R. *Polymer* **2012**, *53*, 569.
41. Rubinstein, M.; Colby, R. H. In Polymer Physics; Oxford University Press: New York, **2003**; Chapter 8, p 309.
42. Yasuda, K. Investigation of the Analogies between Viscometric and Linear Viscoelastic Properties of Polystyrene Fluids. PhD Thesis, Massachusetts Institute of Technology. Cambridge, MA, **1979**.
43. McKee, G. E.; Kistenmacher, A.; Goerrissen, H.; Breulmann, M. In Modern Styrenic Polymers: Polystyrenes and Styrenic Copolymers; Scheirs, J., Priddy, D. B., Eds.; Wiley: West Sussex, **2002**; p 341.
44. Bose, S.; özdilek, C.; Leys, J.; Seo, J. W.; Wübbenhorst, M.; Vermant, J.; Moldenaers, P. *Appl. Mater. Interfaces* **2010**, *2*, 800.
45. Mu, M. F.; Walker, A. M.; Torkelson, J. M.; Winey, K. I. *Polymer* **2008**, *49*, 1332.
46. Grossiord, N.; Kivit, P. J. J.; Loos, J.; Meuldijk, J.; Kyrylyuk, A. V.; van der Schoot, P.; Koning, C. E. *Polymer* **2008**, *49*, 2866.
47. Grunlan, J. C.; Kim, Y. S.; Ziaee, S.; Wei, X.; Abdel-Magid, B.; Tao, K. *Macromol. Mater. Eng.* **2006**, *291*, 1035.
48. Coleman, J. N.; Khan, U.; Blau, W. J.; Gun'ko, Y. K. *Carbon* **2006**, *44*, 1624.
49. Coleman, J. N.; Cadek, M.; Blake, R.; Nicolosi, V.; Ryan, K. P.; Belton, C.; Fonseca, A.; Nagy, J. B.; Gun'ko, Y. K.; Blau, W. *J. Adv. Funct. Mater.* **2004**, *14*, 791.
50. Lin, B.; Sundararaj, U.; Pötschke, P. *Macromol. Mater. Eng.* **2006**, *291*, 227.
51. Lau, K.-T.; Hui, D. *Carbon* **2002**, *40*, 1605.
52. Bubert, H.; Haiber, S.; Brandl, W.; Marginean, G.; Heintze, M.; Bruse, V. *Diamond Relat. Mater.* **2003**, *12*, 811.
53. Schadler, L. S.; Giannaris, S. C.; Ajayan, P. M. *Appl. Phys. Lett.* **1998**, *73*, 3842.
54. van Gurp, M.; Palmen, J. *Rheol. Bull.* **1998**, *67*, 5.
55. Trinkle, S.; Friedrich, C. *Rheol. Acta* **2001**, *40*, 322.
56. Hu, M.; Xia, Y.; McKenna, G. B.; Kornfield, J. A.; Grubbs, R. H. *Macromolecules* **2011**, *44*, 6935.
57. Dorgan, J. R.; Knauss, D. M.; Al-Muallem, H. A.; Huang, T.; Vlassopoulos, D. *Macromolecules* **2003**, *36*, 380.
58. Blackwell, R. J.; Harlen, O. G.; McLeish, T. C. B. *Macromolecules* **2001**, *34*, 2579.
59. Minko, S. *J. Macromol. Sci. Polym. Rev.* **2006**, *46*, 397.
60. Kapnistos, M.; Vlassopoulos, D.; Roovers, J.; Leal, L. G. *Macromolecules* **2005**, *38*, 7852.
61. Doi, M.; Edwards, S. F. In The Theory of Polymer Dynamics; Oxford University Press: New York, **1988**.
62. Kapnistos, M.; Koutalas, G.; Hadjichristidis, N.; Roovers, J.; Lohse, D. J.; Vlassopoulos, D. *Rheol. Acta* **2006**, *46*, 273.
63. Roovers, J.; Graessley, W. W. *Macromolecules* **1981**, *14*, 766.
64. Hodgson, D. F.; Amis, E. J. *J. Chem. Phys.* **1991**, *94*, 4581.
65. Inkson, N. J.; Graham, R. S.; McLeish, T. C. B.; Groves, J.; Fernyhough, C. M. *Macromolecules* **2006**, *39*, 4217.
66. Wang, B.; Sun, G.; He, X.; Liu, J. *Polym. Eng. Sci.* **2007**, *47*, 1610.
67. Sathyanarayana, S.; Olowojoba, G.; Weiss, P.; Caglar, B.; Pataki, B.; Mikonsaari, I.; Hübner, C.; Henning, F. *Macromol. Mater. Eng.* **2013**, *298*, 89.
68. Jonscher, A. K. *Nature* **1977**, *267*, 673.
69. Bose, S.; Bhattacharyya, A. R.; Khare, R. A.; Kamath, S. S.; Kulkarni, A. R. *Polym. Eng. Sci.* **2011**, *51*, 1987.
70. Pötschke, P.; Dukin, S. M.; Alig, I. *Polymer* **2003**, *44*, 5023.
71. Dai, K.; Xu, X. B.; Li, Z. M. *Polymer* **2007**, *48*, 849.